Molecular Catalysis 488 (2020) 110922

Contents lists available at ScienceDirect

Molecular Catalysis

journal homepage: www.elsevier.com/locate/mcat

Catalytic oxidation of cyclohexene by supported gold nanoclusters synthesized in a two-liquid phases system containing eucalyptus essential oil

J. Agúndez, C. Ares, C. Márquez-Álvarez, J. Pérez-Pariente*

Instituto de Catálisis y Petroleoquímica (ICP-CSIC), C/Marie Curie 2, 28049 Cantoblanco, Spain

ARTICLE INFO

Keywords:
Gold nanoclusters
Oxidation
Cyclohexene
Eucalyptus oil
SBA-15

ABSTRACT

Gold nanoclusters (d < 1 nm) have been synthesized in a two-liquid phases system, the aqueous phase being formed by dissolving gold in a solution of ammonium chloride in concentrated nitric acid (1: 4, w/w), while eucalyptus essential oil is the organic phase. The mesoporous SBA-15 material functionalized with mercaptopropyl groups (after surfactant removal: d_p = 6.3 nm, 3.5 wt% S) was contacted with aliquots of the Au-containing essential oil phase taken at 1, 3, 6 and 8 days of contact time between both phases. In this way, gold was immobilized on the support, ranging from 0.4 wt% for the 1-day sample, to 2.7 wt% in the 3-days material. UV–vis spectra show the presence of gold nanoclusters in these samples, but the surface plasmon resonance at 520 cm^{-1}, characteristic of Au nanoparticles, was not detected save for the 3-days sample. ^{13}C MAS NMR and TG evidence that the thiol groups of the support remain mostly unaltered for the 1-day sample, but oxidation to sulfonic acid groups becomes apparent for contact time > 3 days, and reaches nearly 60 % of the total sulphur species after 8 days of contact time as estimated from XPS analysis. The Au-SH-bearing catalyst is inactive for cyclohexene oxidation with molecular oxygen in liquid phase, but those having sulfonic groups are active and selective for its allylic oxidation. It has been found for the 8-day catalyst that the gold nanoclusters partially evolve spontaneously in the reaction medium to form gold nanoparticles, and this agglomeration process parallels the increase in catalyst activity.

1. Introduction

Metal nanoparticles and clusters are attracting an increasing interest for catalytic applications for their unique properties in important chemical and energy-related processes (see references [1–3] for very recent developments in this area). More specifically, gold nanoparticles (AuNPs) are able to catalyze a large number of chemical reactions, among them the selective oxidation of organic molecules [4,5]. The catalytic performance of the AuNPs in these reactions is related, among other factors, to their size and morphology, which in turn are dependent upon their synthesis pathway. Hence, this has prompted intensive research in designing new synthesis methodologies that aimed not only at the control of these two properties, but also to cope with sustainability aspects of the synthesis process. On this regard, increasing attention is being devoted to environmental benign routes, and in particular to the use of substances derived from plants that can play both the role of reduction of the gold precursors and capping agents of the nascent AuNPs. Following this approach, a large number of plant extracts have been used, rendering AuNPs of different sizes and morphologies, usually in the 10 − 50 nm range [6–9]. In the vast majority of these methods, aqueous extracts of plants are mixed with diluted aqueous solutions of $HAuCl_4$, in such a way that the formation of the AuNPs takes place in the aqueous solution that contains a variety of complex soluble biomolecules derived from the plant extract. These biomolecules are responsible for the reduction of Au(III) to Au(0) and the stabilization of the resulting Au NPs. In very few reports essential oils are also used [10–12], but even in these cases the oils are mixed with ethanol/water mixtures [10,11] or acetone [12] and then a small portion of the resulting solution is added to the aqueous $HAuCl_4$ solution, in such a way that a water-rich, single liquid phase system is again formed. Typically, the concentration of the essential oil in these solutions is 1 % (v/v) [11].

Far from these one-liquid phase methods, a new two-liquid phases approach has been developed based on the use of water-insoluble essential oils as organic phase, and a gold water solution formed by dissolving gold lumps in an ammonium chloride solution in concentrated nitric acid (this solution is a variety of the well-known *aqua regia*, usually prepared by mixing nitric and hydrochloric acids, 1:3 mol ratio) as aqueous phase [13,14]. The development of this procedure has been inspired by historical eighteenth century recipes to prepare the so-

* Corresponding author.
E-mail address: jperez@icp.csic.es (J. Pérez-Pariente).

https://doi.org/10.1016/j.mcat.2020.110922
Received 16 December 2019; Received in revised form 6 March 2020; Accepted 23 March 2020
Available online 13 April 2020
2468-8231/

called potable gold, then a reputed medicine with a longstanding tradition that was nevertheless forgotten in nineteenth century [15,16]. Following this procedure and by using rosemary (*Rosmarinus officinalis*) essential oil, a mixture of gold nanoparticles (1 − 8 nm) and small nanoclusters are formed in the oil phase at high concentration of gold in the aqueous phase [13]. However, if the concentration is reduced, only gold nanoclusters are obtained [14]. Moreover, these gold nanoclusters can be conveniently immobilized on ordered mesoporous materials (SBA-15) functionalized with thiol groups, and the resulting solids behave as selective catalysts for the allylic oxidation of cyclohexene with molecular oxygen in mild, liquid phase conditions [14].

The reduction of metal and the subsequent stabilization of the nascent gold entities carried out by crude plant derivatives is a complex chemical phenomenon that involves several biomolecules therein present [17]. On this regard, nearly thirty different individual molecules have been identified in rosemary essential oil, being 1,8-cineol (24.9 wt %), camphor (20.9 wt%) and alfa-pinene (21.9 wt%) the three more abundant compounds [13]. Hence, it could be reasoned that the specific chemical composition of the essential oil would have an impact on the resulting gold entities. Based on this hypothesis, we have explored in this work the synthesis of gold entities by using the two-liquid phase system described above by replacing the rosemary essential oil by eucalyptus (*Eucalyptus globulus*) essential oil. The qualitative composition of this oil is closely related to that of rosemary, but the content of cineol is much higher (55 wt%), as well as that of alfa-pinene, but to a lesser extent (22 wt%), while no camphor is detected and the concentration of the remaining components is < 4 wt% (see below). As it has been discussed above, the use of rosemary oil can lead to AuNPs or gold nanoclusters depending on the synthesis conditions. Therefore, a suitable support for their immobilization should have the appropriated textural properties (large surface area and pore volume) and in particular pores with diameter large enough to accommodate these gold entities. These requirements are satisfied by ordered mesoporous materials [18], and in particular by SBA-15 functionalized with thiol groups, which have been successfully used previously to immobilize gold nanoclusters prepared by using rosemary oil [14]. In the present work, the metal clusters have also been immobilized on the mesoporous SBA-15 material functionalized with mercaptopropyl moieties and the resulting solids used as catalysts for the liquid phase oxidation of cyclohexene with oxygen at atmospheric pressure.

2. Experimental

2.1. Synthesis of thiol-containing SBA-15

Propyl-thiol mesoporous SBA-15 was prepared from a gel with molar composition: 1.0 TEOS:0.111 MPTMS:0.0186 P123:6.42 HCl:180 H_2O, where TEOS stands for tetraethyl orthosilicate (Sigma-Aldrich, > 99 %); MPTMS for (3-mercaptopropyl)trimethoxysysilane (Sigma-Aldrich, 95 %); P123 for Pluronic 123, the triblock co-polymer $PEO_{20}PPO_{70}PEO_{20}$, m.w. ~5800 (Sigma-Aldrich); and HCl for hydrochloric acid (Panreac, 37 wt%), following the procedure described in ref [14]: 125 mL of 1.9 M HCl were placed in a 500 mL plastic bottle provided with a cover having a hole for the insertion of a PTFE (Polytetrafluoroethylene) stirrer blade, and 4 g of P123 were added. Then, the bottle was heated at 40 °C in a silicone oil bath, and 8.2 mL of TEOS were added. After 45 min, 764 μL of MPTMS were added, and the mixture was stirred for 22 h. After that, it was poured into a stainless-steel autoclave provided with a Teflon liner, and heated statically at 100 °C for 24 h. The autoclave was then cooled and its content filtered, washed with ethanol and dried at room temperature overnight. The dried sample was treated with ethanol (200 mL of ethanol per g of sample) under stirring in a 1 L round-bottom flask at 90 °C for 24 h in order to remove the surfactant. The resulting sample is denoted as E-ext.

2.2. Synthesis of the gold nanoclusters

Gold nanoclusters were prepared from a two-liquid phases system according to a procedure previously described [13,14]. A gold lump (0.1507 g, Johnson-Matthey, 99.99 %) was dissolved under gentle stirring in 48.2 g of *aqua regia*, prepared by mixing (4:1, w/w) nitric acid (Panreac, 65 wt%) and ammonium chloride (Sigma-Aldrich, > 98 wt%), while heating at 40 °C in a sand bath. This solution has a 1:320 gold-to-*aqua regia* weight ratio. After cooling, the resulting golden yellow solution was distributed in two 50 mL decanting funnels, and then 12 g of eucalyptus essential oil were gently added to each of them, where it remains as a top layer over the gold solution. The system is then left at room temperature undisturbed, i.e., the two liquid phases are not mixed, and aliquots of the organic layer are taken at selected time intervals to prepare the Au-SBA-15 materials, as it is described below. The area of the contact surface between both liquid phases was 10.7 cm^2. The eucalyptus essential oil (*Eucalyptus globulus*) was supplied by the Spanish company El Granero Integral (The Integral Barn) and has the following chemical composition (wt. %) as determined by GC–MS employing a gas chromatograph (Agilent 6890) coupled with a mass spectrometer (Agilent 5973 N) using a capillary column made of methylpolysiloxane (30 m x0.25 mm x0.25 μm), heating from 70 to 290 °C at 6 °C /min: 55.1 % 1,8-cineole, 22.3 % *alpha*-pinene, 3.8 % p-menthenyl acetate, 2.2 % allo-aromadendrene, 2.2 % *alpha*-terpineol, 2.2 % trans-pinocarveol, 2.1 % *p*-cymene, 0.6 % phellandrene, 0.6 % *beta*-pinene, 0.5 % 4-terpineol, 0.3 % borneol, 0.3 % myrcene, 0.1 % camphene (see Fig. S1 of Supplementary Information for the molecular structure of the three most abundant compounds).

2.3. Immobilization of the gold nanoclusters on SBA-15

Aliquots of 3.75 mL of the organic layer were taken after 1, 3, 6 and 8 days of the addition of eucalyptus oil and each of them was mixed with 18.75 mL of ethanol. To this solution 0.500 g of the extracted SBA-15 material were added and the mixture was stirred at room temperature for 3 h. After that, the solid was separated by centrifugation and washed with four portions of 40 mL each of ethanol. The corresponding samples were denoted as Ex, x = 1, 3, 6 and 8, as shown in Scheme 1.

2.4. Characterization techniques

Powder X-ray diffraction was carried out using a PANalytical X'pert Pro instrument (Cu Kα radiation). Gold content of the solid was determined by inductively coupled plasma (ICP-OES) spectrometry with an ICP Winlab Optima 3300 DV Perkin-Elmer spectrometer. Thermogravimetric analyses were performed in a Perkin-Elmer TGA7 instrument, in air (40 mL/min) with a 20 °C/min heating ramp from 25 to 900 °C. CHNS elemental analyses were done in a LECO CHNS-932 analyser provided with an AD-4 Perkin-Elmer scale. Nitrogen adsorption-desorption isotherms where measured in a Micromeritics ASAP 2420 apparatus at the temperature of liquid nitrogen (-196 °C). The samples were degassed in situ at 70 °C in vacuum for 16 h prior to analysis. Surface area was determined using the BET method. The pore volume and the average pore diameter were calculated by applying the BJH protocol to the adsorption branch of the isotherm. Diffuse reflectance UV–vis spectra were recorded on a Cary 5000 Varian spectrophotometer equipped with an integrating sphere with the synthetic polymer Spectralon as reference. The data were expressed according to the Kubelka-Munk function. MAS NMR spectra were recorded with a Bruker AV 400 WB spectrometer. ^{1}H to ^{13}C cross-polarization (CP) spectra were recorded using a $\pi/2$ rad pulses of 4.5 μs for ^{1}H, a contact time of 5 ms and a recycle delay of 3 s. For the acquisition of the ^{13}C spectra, the samples were span at a rate of 5–5.5 kHz. ^{29}Si MAS NMR spectra were recorded in a 4 mm probe at 79.5 MHz.

Transmission electron microscopy studies were carried out using a JEOL 2100 F electron microscope operating at 200 kV in conventional

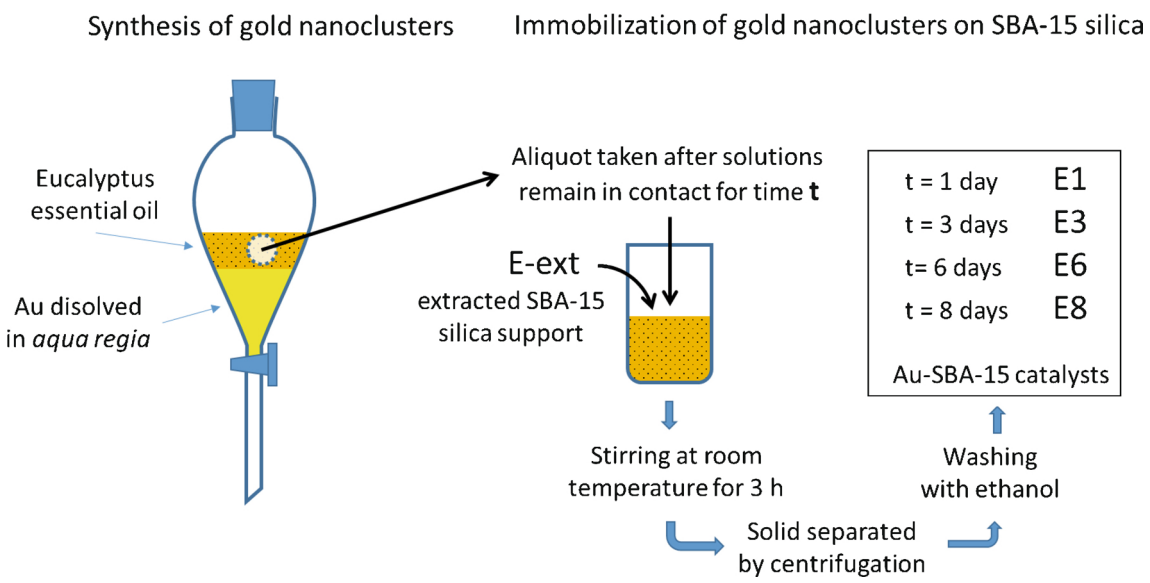

Scheme 1. Synthesis of SBA-15 silica-supported gold catalysts.

and STEM/HAADF mode. The catalysts were dispersed in ethanol and dropped onto a holey carbon copper grid for the observations. X-ray photoelectron spectra (XPS) have been collected using a SPECS instrument with UHV system (pressure in the range of 10^{-10} mbar), equipped with a PHOIBOS 150 9MCD energy analyzer. A non-monochromatic Mg K_α (1253.6 eV) X-ray source was used, working at a power of 200 W, with an acceleration voltage of 12 kV. High-resolution regions were recorded with a pass energy of 20 eV. For analysis, the powder samples were pressed into self-supporting wafers and stuck on the sample holder with double-sided adhesive conductive carbon tape. Spectra were referenced against the O 1s emission line (binding energy set to 532.9 eV) to correct for charging effect. Decomposition of experimental peaks into components (70 % Gaussian, 30 % Lorentzian) was done using a non-linear, least squares fitting algorithm and a Shirley baseline. Relative atom ratios were calculated from the sum area of the core-level components of Si, S and Au, using the relative sensitivity factors provided by Casa XPS software.

2.5. Catalytic tests

The oxidation of cyclohexene with molecular oxygen was carried out by the procedure described in [14], which was developed from that reported in [19]. The catalytic reaction was carried out in a 50 mL four-neck round-bottom glass flask, provided with a condenser through which water at 5 °C was circulated to minimize the evaporation of reagents and products. The flask was immersed in a silicone oil bath to keep the reaction temperature at 65 °C, measured inside the reaction mixture by a thermometer inserted in one of the necks. The experimental set-up was not protected against environmental light. The reaction mixture was made of 0.049 mol of cyclohexene (4.055 g, Sigma-Aldrich, 99 %), 0.4055 g of octane (10 wt% referred to cyclohexene; Sigma-Aldrich, > 99 %), 0.2027 g of a ter-butyl hydroperoxide solution (TBHP, 5 wt% referred to cyclohexene; ~ 5.5 M in decane, Sigma-Aldrich), 3.041 g of toluene (75 wt% of the cyclohexene; Panreac, > 99.5 %), and 0.050 g of catalyst. O_2 (1.8 mL/min) was bubbled through the stirred reaction mixture. The catalysts were previously heated at 100 °C for 1 h in the reaction flask equipped with a tube containing molecular sieve 5A in order to remove the traces of water coming from the catalysts, cooled down to the reaction temperature of 65 °C, and then the reagents were added. The trap was removed and replaced by the condenser before the reaction starts. Aliquots of 0.20 mL of the reaction mixture were taken at given time intervals and analysed by GC in a Varian CP-300 instrument, by using a FactorFour™ (Varian VF-1 ms) dimethylpolysiloxane capillary column of 15 m of length and 0.25 mm of i. d. Octane was used as internal standard. Five reaction products were identified; two of them resulting from the addition of oxygen to the cyclohexene double bond, namely cyclohexene epoxide and cyclohexanediol, and three coming from the allylic oxidation of the cyclohexene ring: 2-cyclohexen-1-ol, 2-cyclohexen-1-one and 2-cyclohexenyl hydroperoxide. Cyclohexene conversion was calculated from the yields of these five products.

3. Results and discussion

3.1. Extracted SH-SBA-15 sample

The synthesis procedure of the SH-SBA-15 material has been described in the experimental section. Both the as-made and the extracted (the surfactant-free product recovered after ethanol extraction) samples show the X-ray diffraction pattern characteristic of well-ordered SBA-15 mesoporous materials, with d_{100} = 9.5 nm and unit cell size a_0 = 11.0 nm for the extracted one (Fig. S2 and Table 1). The nitrogen adsorption/desorption isotherm (Fig. S3) is also characteristic of SBA-15 materials, with surface area and pore volume of about 600 m^2/g and 0.67 cm^3/g, respectively. The pore diameter is 6.3 nm, close to that reported for mercaptopropyl-functionalized SBA-15 materials [20], but clearly smaller than that of pure SBA-15 materials, which is usually around 7 nm [21]. This reduction of pore size can be attributed to the presence of organosilane propylthiol groups attached to the surface of the SBA-15 channels. Moreover, the chemical analysis reveals the presence of both sulphur and carbon in the sample (Table 2), with a Si/S ratio of 10.6, i.e., nearly 10 % of the Si atoms in the structure are attached to one mercaptopropyl moiety. A more direct evidence of the actual occurrence of the co-condensation process of MPTMS and TEOS and the consequent presence of propylthiol groups in the solid is

Table 1
Structural and textural properties of SH-SBA-15 support and catalysts.

Sample	Unit cell parameter a_0 (nm)	S_{BET} (m^2/g)	Pore volume (cm^3/g)	Pore size (nm)
E-ext	11.0	603	0.67	6.3
E1	10.9	381	0.48	5.6
E3	11.0	395	0.47	5.5
E6	10.9	318	0.43	5.6
E8	10.9	296	0.42	5.6

Table 2
Chemical composition (wt%) and TG results of the SH-SBA-15 support (E-ext) and catalysts.

Sample [a]	C	H	S	Au	C/S [b]	S/Au [b]	%Weight loss T > 140 °C
E-ext	13.9	3.2	3.5	–	10.5	–	24.1
E1	16.9	3.4	3.3	0.4	13.6	52	27.9
E3	12.2	3.0	3.3	2.7	9.9	7.5	20.6
E6	13.2	3.0	3.3	2.6	10.7	7.8	22.2
E8	15.1	3.2	3.2	2.1	12.6	9.3	26.3

[a] Traces of N are found in the samples ranging in increasing order from 0.1 wt% for E1 to 0.4 wt% for E8.
[b] Atomic ratio.

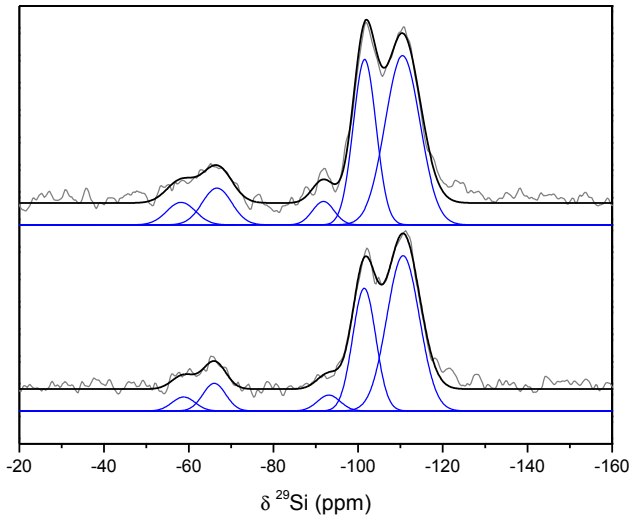

Fig. 1. ^{29}Si MAS NMR spectra of the extracted E-ext (top) and Au-containing E8 (bottom) samples. Deconvolution of spectra into five Q^n and T^m components is also shown.

Table 3
Chemical shift and peak area percentage of Q^n and T^m silicon species determined by deconvolution of ^{29}Si MAS-NMR spectra.

Sample	Chemical shift (ppm)					Peak area (%)				
	Q^2	Q^3	Q^4	T^2	T^3	Q^2	Q^3	Q^4	T^2	T^3
E-ext	−92	−102	−111	−58	−67	4.3	31.7	49.5	5.4	9.1
E8	−93	−101	−111	−59	−66	3.9	30.8	55.0	3.5	6.8

provided by ^{29}Si MAS NMR of sample E-ext (Fig. 1). Two different sets of signals are observed in the spectrum. Three resonances are found at −92 (weak), −102 and −111 ppm, assigned to Q^2, Q^3 and Q^4 species, respectively, where Q^n refers to $[Si(OSi)_n(OH)_{4-n}]$ environments, with n = 0, 1, 2, 3 and 4. The high intensity of the signal at −102 ppm, which accounts for 37 % of total area of Q^n signals (Table 3), evidences the high concentration of silanol Si−OH groups present in the sample. It should be noted, nevertheless, that an undetermined fraction of these silanol species would actually correspond to Si-ethoxy moieties, as proven by ^{13}C CP/MAS NMR (see below). A second group of signals appears at −67 and −58 ppm, being the former more intense than the latter. These signals, which account for 14.5 % of total Si species, are attributed respectively to T^3 and T^2 sites, where T^m corresponds to silane species (those having C-Si bonds) in environments described as $[RSi(OSi)_m(OH)_{3-m}]$, m = 0, 1, 2 and 3 [22], confirming in this way that the MPTMS is indeed forming part of the silica framework located at the channel surface, in agreement with the observed reduction of the average pore size reported above. Further confirmation of the presence of mercaptopropyl moieties in the sample is provided by the

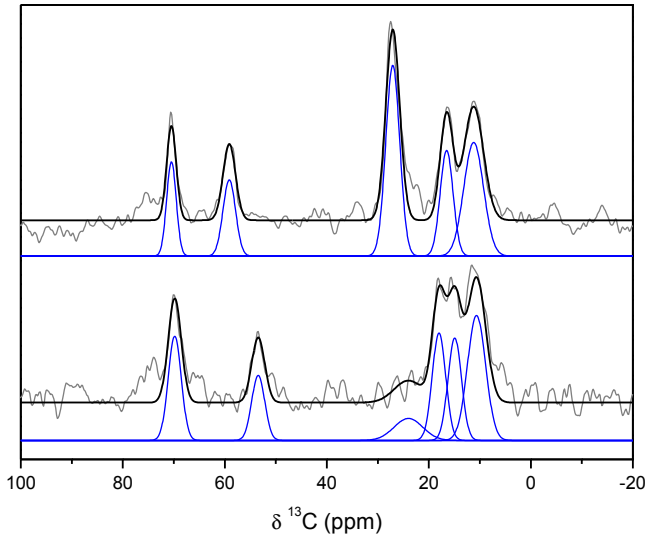

Fig. 2. ^{13}C{^{1}H}CP/MAS NMR spectra of extracted E-ext (top) and Au-containing E8 (bottom) samples. Spectral deconvolution is shown to highlight the location of relevant resonance peaks of the anchored functional groups as discussed in the text.

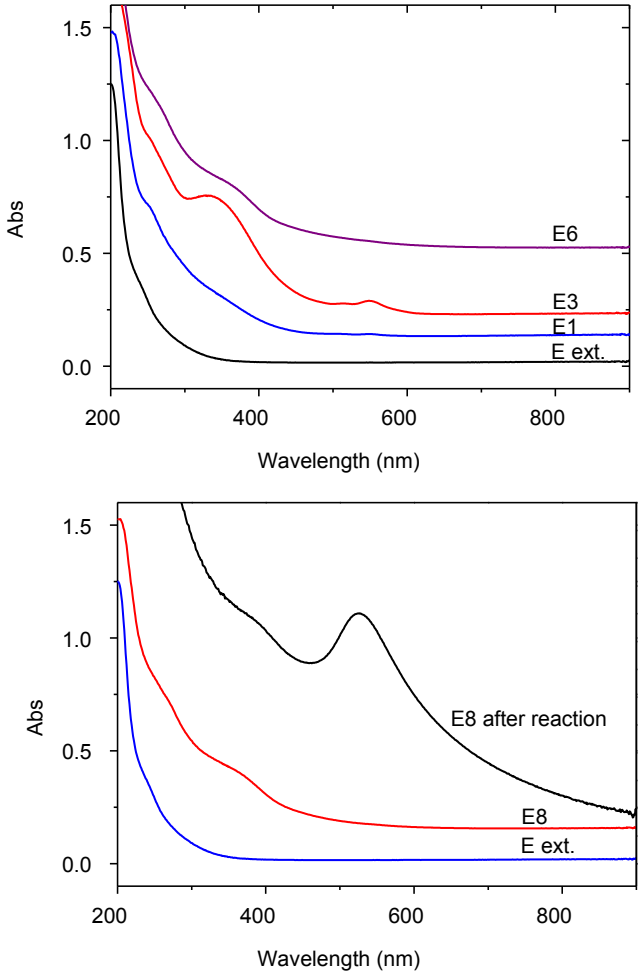

Fig. 3. UV–vis spectra of the Au-containing samples.

^{13}C{^{1}H}CP/MAS NMR spectra shown in Fig. 2. The intense resonance at 27 ppm is contributed by the α carbon, adjacent to the SH group, as well as by the carbon atom in β position, while that at 11 ppm arises

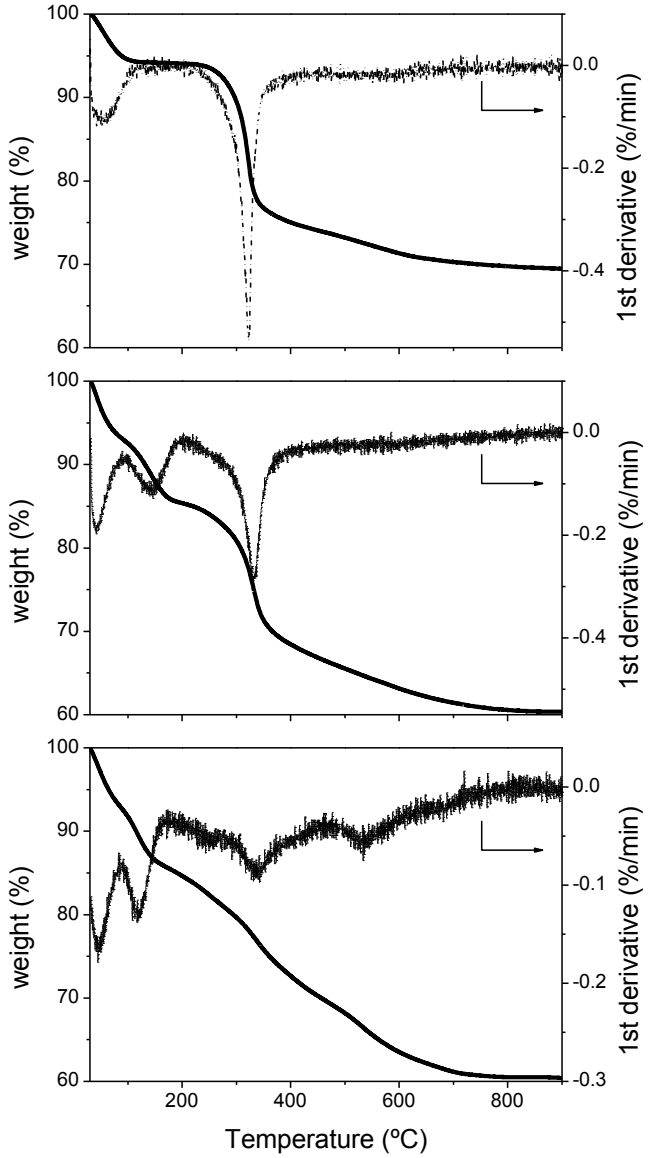

Fig. 4. TG/DTG curves of the extracted support E-ext (top) and Au-containing samples E1 (middle) and E8 (bottom).

from the γ carbon, which is attached to the Si atom in the silane [23,24]. The two signals at 16 and 59 ppm are attributed respectively to the methyl and methylene carbon atoms of the ethoxy groups ($-O-CH_2-CH_3$), which are formed by reaction of silanol groups present in the material with hot ethanol during the extraction process [23,24]. Finally, the signal at 70 ppm would correspond to the methylene carbon atoms adjacent to ether oxygen atoms of residual P123 surfactant that remains in the material after the extraction process [23]. According to this assignment, the surfactant methyl groups would also contribute to the intensity of the peak at 16 ppm. The presence in the sample of these carbon-bearing chemical species in addition to mercaptopropyl silane explains that the C/S atom ratio recorded in Table 2 is higher than that expected for the S-bearing organic moiety.

3.2. Gold-containing samples

Au entities present in the eucalyptus oil phase were immobilized on the SH-SBA-15 extracted material by following the procedure described in the experimental section, subsection 2.3. The unit cell size of the materials recovered after contacting the extracted SH-SBA-15 sample with the eucalyptus essential oil/ethanol solution is quite similar to that of the extracted one (Table 1). Surface area and total pore volume of the Au-containing materials are smaller than those of the SH precursor, while pore size is slightly reduced (Table 1).

The amount of gold present in the samples raises from 0.4 wt% for the material prepared from the eucalyptus oil phase that was in contact with the gold solution for one day (sample E1), to 2.7 wt% for the 3-days sample (E3), and then decreases slightly for longer contact time (Table 2). This decrease can be attributed to a precipitation of part of the gold from the eucalyptus oil solution, because gold crystals are found on the inner wall of the decanting funnel around the interphase between both liquid phases as the contact time is prolonged beyond 3 days. The amount of gold in the 1-day sample is twice that found for a similar preparation procedure and contact time previously reported by using rosemary essential oil [14], which is 0.19, evidencing the higher efficiency of the eucalyptus oil for transferring gold from the *aqua regia* to the oil phase. This behaviour should arise from differences in the respective chemical composition of the two oils, and in particular to the concentration of 1,8-cineole present in the eucalyptus oil, which is nearly twice that of rosemary oil. On this regard, the efficiency of black cardamom aqueous extracts to reduce gold when added to tetrachloroauric solutions has been attributed to the high content (65 wt%) of 1,8-cineole of this plant [25]. In the same way, *Eucalyptus oleosa* leaf aqueous extracts, also rich in 1,8-cineole, have been reported to reduce Au^{3+} from tetrachloroauric solutions [26]. However, in these two cases, gold nanoparticles were obtained, in contrast to the gold nanoclusters formed following the procedure reported here, as it will be discussed below.

The amount of S in the Au-containing samples is close to that of the extracted gold-free support, although the Au deposition procedure leads to a slight (< 10 %) loss of sulphur (Table 2). Partial removal of mercaptopropyl groups attached to the silica support upon contact with the *aqua regia* solution of gold is also confirmed by ^{29}Si MAS NMR. As shown in Table 3, the amount of T^m species (silane groups) determined from the ^{29}Si MAS NMR spectrum of sample E8 (Fig. 1), accounts for 10.3 % of total silicon species. This result corresponds to a decrease of silane groups of 29 % respect to sample E-ext, indicating that silane removal might be higher than expected according to the decrease of bulk sulphur content determined by chemical analysis. Chemical analyses show that the S/Au ratios attained are in the range $7-52$. The carbon content increases for the E1 and E8 samples, particularly for the former, which suggests that some organic material from the oil phase is incorporated into the solids.

The UV–vis spectra of AuNPs present a characteristic surface plasmon resonance at $\sim 520\,cm^{-1}$ [27]. Moreover, UV–vis bands of gold clusters stabilized with thiol groups and having a metal core size of 0.8 nm have been reported in the range $300-450$ nm [28], while UV bands at $\sim$ 250 nm have been attributed to gold clusters having a partial positive charge [29]. The UV–vis spectra of the Au-containing samples prepared in this work are shown in Fig. 3. Bands of weak intensity are observed at $\sim$ 370 nm and $\sim$ 250 nm, but the band of the plasmon resonance at $\sim$ 520 cm^{-1} characteristic of AuNPs is not detected. An exception to this behaviour is sample E3, the one with the highest Au content, where a band of low intensity at $\sim 550\,cm^{-1}$ with a weak shoulder at $515\,cm^{-1}$ is observed, and a new intense band at 350 nm is detected while that at 370 nm is absent. This result is in strong contrast with the formation of gold nanoparticles of $\sim$ 28 nm of average size when *Eucalyptus oleosa* leaf aqueous extracts are used to reduce Au^{3+} from tetrachloroauric solutions [26]. This evidences the efficiency of the two-liquid phases method based on the use of essential oils to render small gold nanoclusters, in contrast with the AuNPs produced from plant extracts using a single aqueous phase, as it has been discussed above.

Some noticeable differences have been observed between the extracted and the Au-containing samples concerning their thermogravimetric analysis, which have been plotted in Fig. 4. The TG curve of the

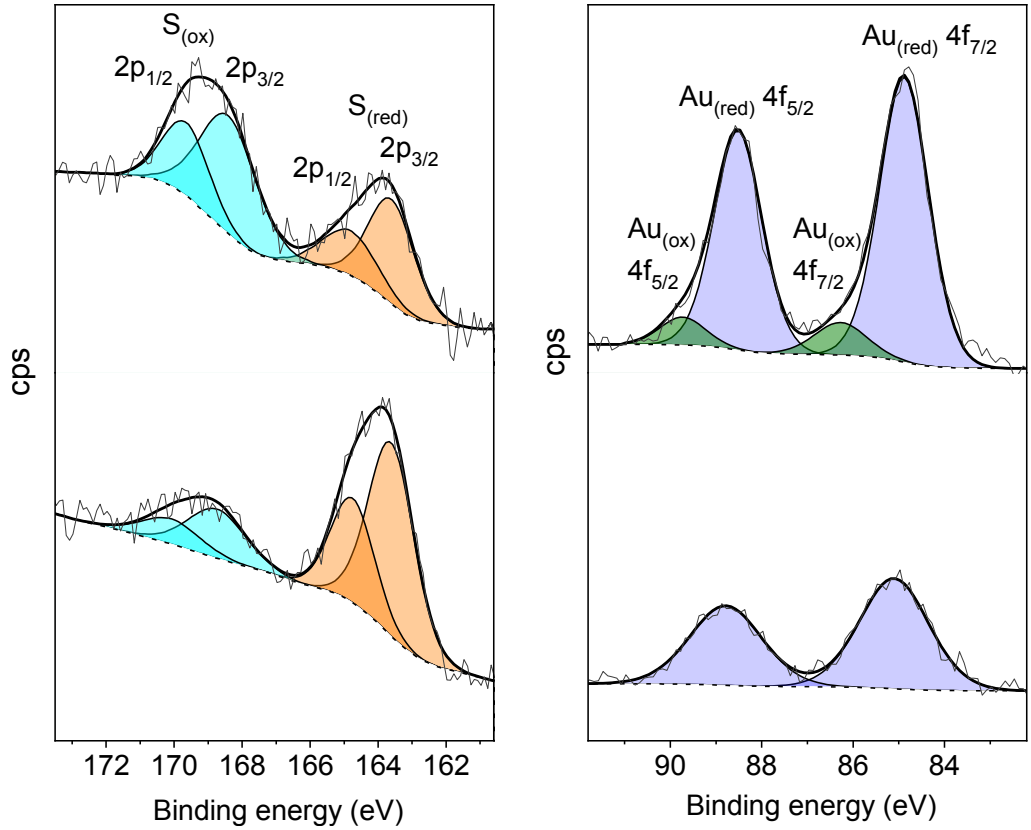

Fig. 5. Deconvoluted S 2p and Au 4f core-level XP spectra of samples E1 (bottom) and E8 (top). Labels indicate the assignment of doublets to reduced sulphur ($S_{(red)}$) and gold ($Au_{(red)}$) and oxidized sulphur ($S_{(ox)}$) and gold ($Au_{(ox)}$) species.

Table 4
XPS characterization data of selected gold-containing samples.

Sample	BE (eV)					Atomic ratio			
	Si 2p	S $2p_{3/2}$	S $2p_{1/2}$	Au $4f_{7/2}$	Au $4f_{5/2}$	S/Si	Au/Si	Au/S	S_{ox}/S [a]
E1	103.5	163.6 168.8	164.8 170.1	85.1	88.8	0.068	0.007	0.103	0.24
E8	103.5	163.6 168.4	164.8 169.7	84.9 86.3	88.5 89.7	0.065	0.014	0.212	0.58

[a] Fraction of oxidized sulphur species.

extracted sample shows a weight loss below 100 °C due to water desorption. A sharp and intense weight loss is observed centred at ~320 °C, which is followed by a continuous and smooth weight loss at T > ~380 °C. This two last thermal events are due basically to the desorption/combustion of the organic material present in the sample, in particular the mercaptopropyl moieties [20,24] and, to some extent, also the remnant surfactant and ethoxy groups detected by NMR. The water desorbed by the condensation of the silanol groups detected by NMR will also contribute to the total weight loss at high temperature.

The TGA of the 1-day sample is quite similar to the extracted one, save for the presence of an additional thermal feature centred at 130 °C, which can be ascribed to the removal of some volatile organic material incorporated from the essential oil phase during the gold deposition process, in agreement with the higher amount of carbon found in this sample compared to the support E-ext (Table 2). The similarity of the TG patterns of the extracted and 1-day samples suggests that the gold deposition process does not modify essentially the nature of the functional groups therein present when the support was in contact with the oil solution obtained after only 1 day of reaction with *aqua regia*. However, the weight loss profile at temperatures above 250 °C, at which the removal of the attached silane groups occur, shows a progressive change for samples prepared with gold solutions obtained after 3 and 6 days of contact time of the oil with the acid solution (samples E3 and E6, respectively), with no further changes found for longer contact time (sample E8). As shown in Fig. 4 for sample E8, these profiles exhibit a weaker and smoother weight loss at ca. 320 °C compared to those of samples E-ext and E1, which leads to a broader peak in the first derivative plot, slightly shifted towards higher temperature (ca. 335 °C). Furthermore, an additional weight loss step appears above 450 °C. The TGA patterns of samples E3, E6 and E8 are quite similar to those previously reported for analogous materials synthesized from rosemary oil [14] and also for mesoporous materials bearing oxidized mercaptopropyl groups [24]. Indeed, it has been shown that the decomposition of alkyl-sulfonic acid groups anchored on SBA-15 by direct synthesis takes place at 450 °C [20]. Therefore, our TGA results suggest that part of the mercaptopropyl groups are oxidized during the gold deposition process if the contact time between the eucalyptus oil and the gold-containing *aqua regia* solution is prolonged for at least 3 days.

A more direct evidence of the actual oxidation of thiol to sulfonic groups is given by the ^{13}C CP/MAS NMR spectrum of the 8-days sample (Fig. 2), which shows resonances at 11, 18 and 54 ppm that can be assigned, respectively, to methylene carbons attached to Si, and those

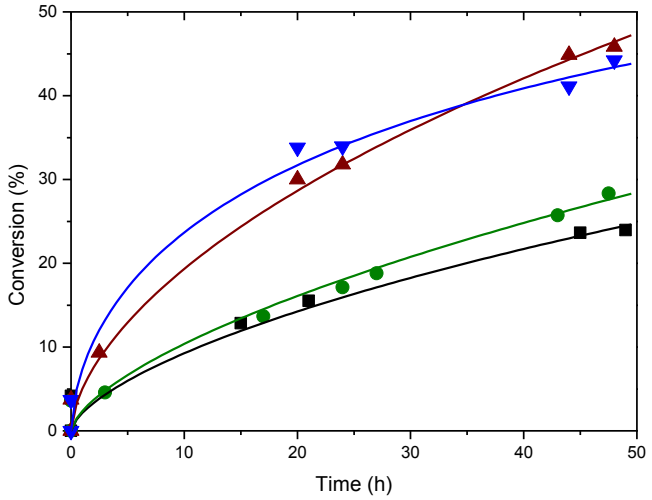

Fig. 6. Conversion of cyclohexene as a function of time for the gold-free support E-ext (black squares) and gold catalysts E1 (green circles), E3 (brown up triangles) and E8 (blue down triangles). Solid lines have been drawn as visual aid only.

in β and α positions respect to the $–SO_3H$ moiety in propylsulfonic groups [22]. Other signals found at 70 and 15 ppm, that were present also in sample E-ext, are assigned to residual P123 species [23], which do not seem to be affected by the gold impregnation treatment. However, this treatment removes the ethoxy groups present in the extracted material, as the corresponding NMR signals have vanished. It can be noticed that the signal detected at 27 ppm, corresponding to carbon atoms attached to the –SH moiety, exhibits much lower intensity compared to sample E-ext, and, on the other hand, no signals of disulphide bridges arising from the eventual condensation of thiol groups (signals in the 20 − 50 ppm range) are detected, nor that at 64 ppm attributed to carbon atoms attached to $S(O_2)$ chemical species [23]. Therefore, it can be concluded that, in the case of sample E8 (as well as E6 and, in a lesser extent, sample E3) a large fraction of thiol groups present in the extracted sample are oxidized to sulfonic acid groups during the gold deposition process. This conclusion is further supported by XPS analysis, which provides direct evidence of the chemical state of sulphur. As shown in Fig. 5, the S 2p core-level spectrum of sample E8 exhibits two asymmetric peaks that can be deconvolved into doublets with a characteristic spin-orbit splitting in the range 1.2–1.3 eV and a 2:1 intensity ratio. The low BE doublet, which $2p_{3/2}$ component appears at 163.6 eV (Table 4), can be assigned to thiol while the high BE one (168.4 eV) corresponds to high oxidation state sulphur species such as sulfonate groups [24,30,31]. The spectrum, however, do not show a peak at ca. 162 eV that would be expected for thiol groups bound to gold [30,32], which could be due to the low amount of thiol groups that are interacting with Au because of the low Au loading of the samples. According to the relative areas of both high and low BE peaks, it can be estimated that nearly 60 % of the thiol species were oxidized to sulfonic acid during the gold deposition treatment (Table 4), which is in close agreement with the results of bulk techniques discussed above. It is interesting to notice that the XPS spectrum of sample E1 (Fig. 5) also exhibits both doublets in the S 2p region, although with lower intensity of the high BE peaks, revealing that in this sample oxidation extends to 24 % of thiol groups. This shows that even the oil obtained after only 1 day of contact with *aqua regia* has a certain thiol oxidation capacity. Nevertheless, the oxidation would in this case affect only to thiol groups located on the external surface of the support, for sulfonic acid species are observed when probing the outermost layers of the sample by XPS but they are not detected when using bulk techniques such as TGA and ^{13}C NMR, as discussed above. The results clearly show that the thiol oxidation capacity of the essential oil increases with its contact time with *aqua regia* from 1 to 8 days. Nonetheless, this enhancement of oxidation capacity does not increase significantly the leaching of sulphur. Indeed, according to the S/Si atomic ratios calculated from XPS analysis (Table 4), the decrease of total S concentration of sample E8 respect to sample E1 is below 5%, in agreement with bulk chemical analyses (Table 2).

The oxidation of thiol groups that takes place during the gold deposition treatment can be attributed to the presence of strong oxidant compounds that would be formed in the essential oil in contact with *aqua regia*. This oxidant activity of the essential oil, which becomes apparent specially for contact times of 3 days or longer, should be linked to the changes that we have observed in its colour in that period of time. No changes in colour are detected for the 1-day sample, but the oil starts to acquire a light brown-orange coloration after 3 days, which intensity increases for longer contact times (Fig. S4). These changes strongly suggest that the terpenic compounds initially present in the oil react with the strongly acidic and oxidant solution of gold in *aqua regia*, and the compounds resulting from this reaction (which have not yet been identified) should be able to oxidize thiol to sulfonic groups.

Supported gold species present on the catalysts have been characterized by X-ray photoelectron spectroscopy. The Au 4f core-level spectrum of sample E1 (Fig. 5) exhibits two broad peaks than can be fitted with a single doublet (3:4 intensity ratio) with BE for the Au $4f_{7/2}$ component of 85.1 eV (FWHM = 1.8 eV) and a spin-orbit splitting of 3.7 eV (Table 4). This doublet shows a positive shift of 1.3 eV and a broadening of ca. 0.6 eV respect to spectra reported for Au° nanoparticles within the size range 1 − 3 nm bonded to thiol groups [32,33]. This result is in agreement with the UV–vis spectrum that indicates the lack of Au nanoparticles in this sample, which would contain smaller gold entities. Indeed, it has been shown for supported gold nanoclusters that BE increases respect to bulk 4f core-level as cluster size decreases [34,35]. Furthermore, significant broadening has been observed with decreasing cluster size for clusters of less than 20 atoms. Thus, spectrum of sample E1 suggests that gold would be present as very small clusters in this sample. In is also worth noting that the Au/S atomic ratio calculated for sample E1 from the XPS spectrum (Table 4) is around 5 times higher than the bulk ratio (Table 2), which indicates a noticeable enrichment of gold in the outermost region of the support. Compared to sample E1, the Au 4f spectrum of sample E8 (Fig. 5) shows higher intensity, in agreement with its higher gold content, with a Au/S ratio of ca. 0.2, twice that of sample E1 (Table 4). However, the Au/S ratio of sample E8, is much closer to the bulk ratio, which indicates lower gold surface enrichment in this sample respect to sample E1. Also, the XPS spectrum of sample E8 shows the Au 4f doublet characteristic of Au° nanoclusters slightly shifted to lower BE (84.9 eV for the $4f_{7/2}$ component) and narrower (FWHM = 1.3 eV) in comparison to sample E1. This result indicates that sample E8 would contain larger gold entities, although the high BE supports the absence of nanoparticles. However, it can be clearly seen in Fig. 5 that the Au 4f peaks show some tailing towards high BE and an additional doublet is required for a correct fitting of the spectrum, which accounts for 11 % of total Au 4f peak area. The BE (86.3 eV for the $4f_{7/2}$ component) and spin-orbit splitting (3.4 eV) of this species agree with values reported for Au(III) complexes [36,37] and oxide phases [38–41], indicating that a small fraction of the gold content of sample E8 is present as oxidized Au(III).

3.3. Cyclohexene oxidation

The E1, E3 and E8 samples were tested in the cyclohexene oxidation with molecular oxygen at atmospheric pressure, in the conditions described in the experimental section, and the conversion as a function of the reaction time is plotted in Fig. 6. It can be seen that only for the 3-d and 8-d catalysts the conversion is significantly higher than that of gold-free thiol-containing sample, approaching 40 %–45 % at 48 h of reaction, while the presence of gold in the 1-day sample doesn't enhance the catalytic activity as compared with that of the Au-free

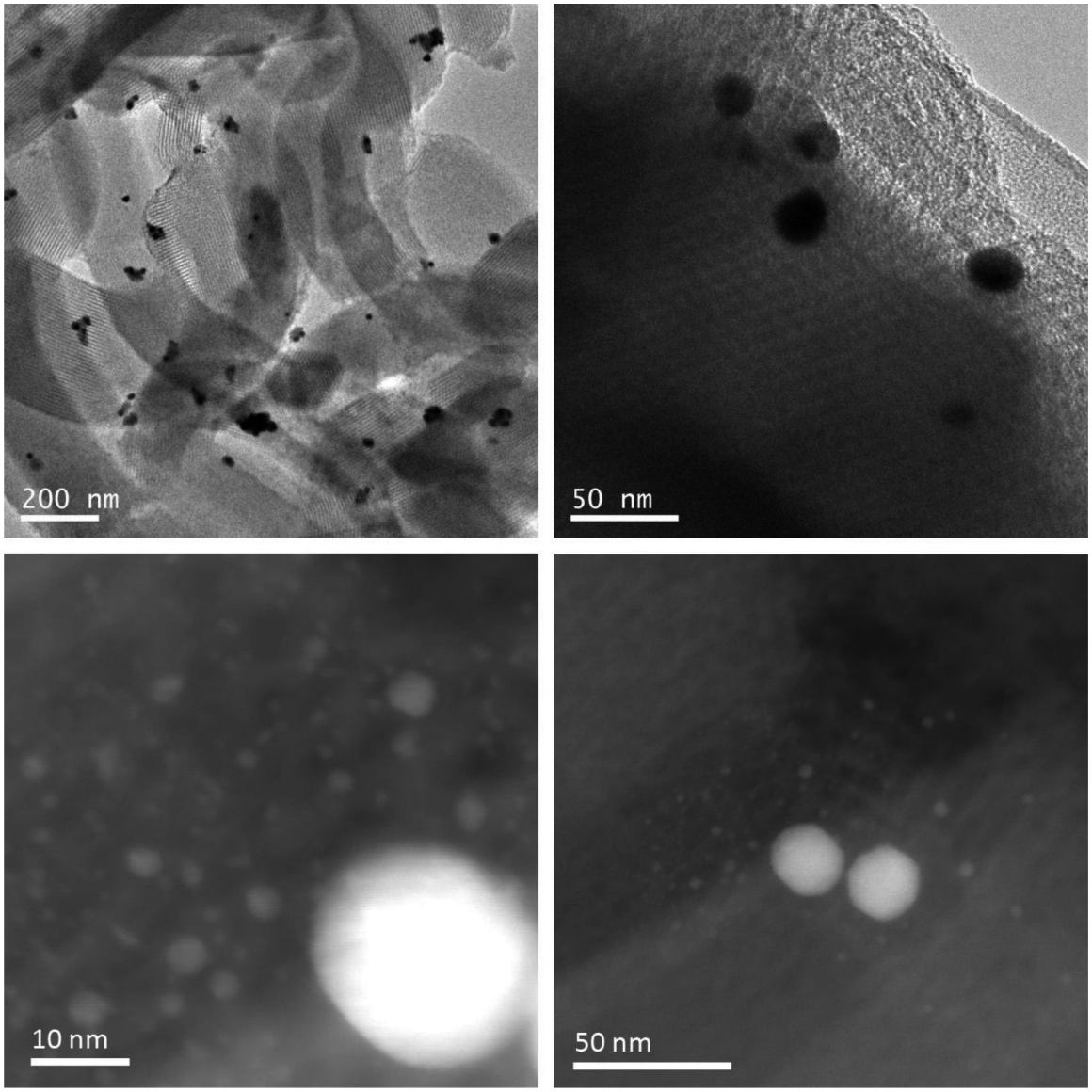

Fig. 7. TEM (top) and STEM (bottom) images of the E8 catalyst after reaction.

material. A similar result has been reported for the 1-day sample prepared by the same method but using rosemary oil [14], and it can be taken as strong evidence that gold nanoclusters attached to thiol groups are essentially inactive for cyclohexene oxidation in the reaction conditions here described, probably due to their high stability. This can be taken as a general conclusion derived from this study at least for the materials and conditions here described. The manifestation of activity by the gold entities present in the E3 and E8 catalysts is therefore linked to the transformation of thiol groups into sulfonic acid groups that occurs during the gold deposition process, as shown by ^{13}C MAS NMR discussed above (Fig. 2). Moreover, it has been observed that the colour of the catalysts changed as the reaction proceeds, from pale yellowish in the pristine state, to pink and then purple. This behaviour suggests that at least part of the gold nanoclusters initially present in the catalysts gradually evolve in the reaction medium to form gold nanoparticles. Indeed, in the UV–vis spectrum of the E8 catalyst after reaction the characteristic plasmon resonance band at $\sim$ 525 cm^{-1} is clearly observed (Fig. 3). However, the two bands associated to the presence of clusters are still detected, although with lower intensity, and a red-shift of the 250 cm^{-1} band to 280 cm^{-1} is observed. This result points to the coexistence in the used catalyst of an ample variety of gold entities, ranging from clusters to nanoparticles. In the TEM images of this sample (Fig. 7) gold nanoparticles with a maximum size of 20 – 25 nm are clearly identified, but the STEM mode allows the detection of abundant much smaller gold entities, some of them with sizes below 1 – 2 nm, about the detection limit of the instrument. The occurrence of this yet incomplete growing process of the gold clusters toward nanoparticles that takes place in the reaction medium has also been observed for catalysts prepared from rosemary oil by following the same procedure here reported [14]. Therefore, there seems to be a positive correlation between catalytic activity and the coalescence of the gold nanoclusters to yield nanoparticles. A similar conclusion has been reported for the same reaction by using silica-supported triphenylphosphine-stabilized Au_9 clusters, which are inactive for the cyclohexene oxidation, much in the same way reported here for the SH-Au clusters [42]. In that case, the catalytic activity is triggered by the formation of Au nanoparticles more than 2 nm in size. In our case, the broad size distribution of gold clusters/nanoparticles present in the catalysts under actual working conditions and their evolution in the reaction medium preclude to establish a clear correlation between the size of gold entities and the catalytic activity. It can be also noticed that the activity of these catalysts is quite close to that prepared from rosemary oil reported in

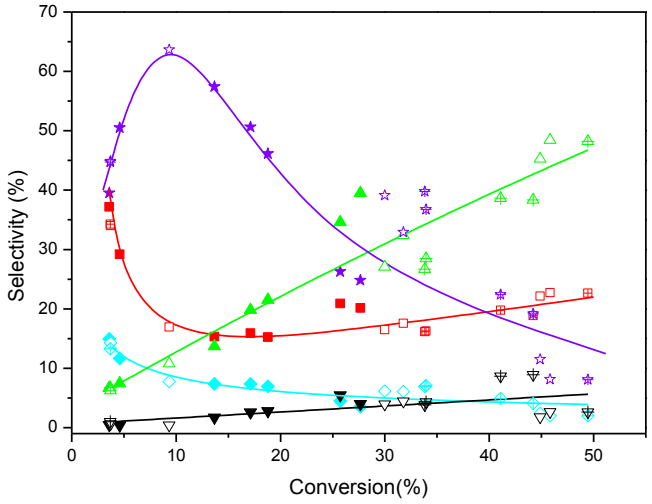

Fig. 8. Selectivity to the reaction products, 2-cyclohexen-1-ol (red squares), 2-cyclohexen-1-one (green up triangles), cyclohexenyl hydroperoxide (violet stars), cyclohexene epoxide (cyan diamonds) and cyclohexanediol (black down triangles), as a function of conversion for catalysts E1 (full symbols), E3 (open symbols) and E8 (crossed open symbols). Solid lines have been drawn as visual aid only.

[14] with a similar Au content (2.57 wt%). This suggests that the intrinsic activity of the gold entities is basically not affected by the nature of the essential oil used in the preparation of the gold nanoclusters.

The selectivity to the several reaction products is plotted in Fig. 8 for all the catalysts as a function of conversion. It can be seen that the three products resulting from the allylic oxidation of the cyclohexene (2-cyclohexen-1-one, 2-cyclohexen-1-ol and 2-cyclohexenyl hydroperoxide) account for nearly 90 % of the total reaction products, and hence the allylic oxidation is a preferred reaction route over the epoxidation of the double bond. Concerning the distribution of products coming from this major route, it can be observed in the figure that the selectivity to 2-cyclohexenyl hydroperoxide is higher than ~50 % for conversion lower than ~20 %, but it decreases rapidly as the conversion increases, and the enone becomes the major product for the Au-containing catalysts as the conversion raises beyond ~30 %. This evolution of the product selectivity with the conversion suggests that the hydroperoxide is transformed into enone and enol as the reaction proceeds. Moreover, it can be observed at conversion < 10 % that both the enol and the hydroperoxide are primary products, but the selectivity to the former decreases rapidly and reaches a minimum at ~ 15 % conversion, and raises slightly beyond that point. On the contrary, the selectivity to hydroperoxide follows an opposite trend, as it increases up to 10 % conversion, and then declines. It can be seen also that the enone is probably a secondary product, but its selectivity steadily increases with conversion, in such a way that the enone/enol ratio increases to 2 as the conversion approaches 45 %. The selectivity pattern of the enone as a function of conversion is quite similar to what has been reported for catalysts prepared from rosemary oil [14], but the evolution of the hydroperoxide and enol at conversion below ~ 10 % differs substantially from those of rosemary oil-derived catalysts.

4. Conclusions

Gold nanoclusters generated in a two-liquid phases system consisting of eucalyptus oil as organic phase and a gold solution in *aqua regia* as aqueous phase can be immobilized in thiol-bearing SBA-15 mesoporous materials, leading to solids with gold loadings in the range 0.4–2.7 wt% as a function of the contact time between the eucalyptus oil and the gold solution, which are higher than those found for catalysts prepared from rosemary oil under similar conditions. This evidences that the eucalyptus oil behaves as a very efficient phase-transfer, reductant and capping agent of the gold entities present in the strongly acidic and oxidant aqueous phase. Upon contacting the gold-rich oil phase with the functionalized support, most of the thiol groups are oxidized to sulfonic acid groups if the contact time between the oil and the aqueous phase is sufficiently long. Gold is present in these materials as very small clusters, and minor amount of Au(III) is present at the longest contact time (8 days). It has been found that as far as the thiol groups remain unaltered, the catalyst is inactive for the oxidation of cyclohexene, which has been attributed to the presence of gold nanoclusters strongly interacting with thiol groups forming probably very stable thiolate configurations. However, the reaction is triggered if the thiol groups are oxidized to sulfonic groups. In this latter case, it has been observed a partial agglomeration of the gold nanoclusters toward gold nanoparticles during the reaction, which seems to be the main responsible for the catalytic activity. The allylic oxidation of cyclohexene is the major catalytic route, where 2-cyclohexenyl hydroperoxide is an intermediate product which evolves to form the stable 2-cyclohexen-1-one and 2-cyclohexen-1-ol, with enone/enol ratio of ~ 2 at high conversion.

CRediT authorship contribution statement

J. Agúndez: Conceptualization, Resources, Investigation, Visualization, Writing - review & editing. **C. Ares:** Investigation. **C. Márquez-Álvarez:** Investigation, Visualization, Writing - review & editing. **J. Pérez-Pariente:** Conceptualization, Methodology, Supervision, Writing - original draft.

Declaration of Competing Interest

The authors declare that there are no conflicts of interest.

Acknowledgements

The authors acknowledge the current Spanish Ministry of Science, Innovation and Universities (formerly the Ministry of Economy and Competitiveness) for the funding of this work through the project MAT2016-77496-R.

Appendix A. Supplementary data

Supplementary material related to this article can be found, in the online version, at doi:https://doi.org/10.1016/j.mcat.2020.110922.

References

[1] K. Kwak, D. Lee, Acc. Chem. Res. 52 (2019) 12–22.
[2] T. Imaoka, K. Yamamoto, Bull. Chem. Soc. Jpn. 92 (2019) 941–948.
[3] S. Sultan, J.N. Tiwari, A.N. Singh, S. Zhumagali, M. Ha, C.W. Myung, P. Thangavel, K.S. Kim, Adv. Energy Mater. 9 (2019) 1900624.
[4] A.S.K. Hashmi, G.J. Hutchings, Angew. Chem. Int. Ed. 45 (2006) 7896–7936.
[5] A. Corma, H. García, Chem. Soc. Rev. 37 (2008) 2096–2126.
[6] A.K. Mittal, Y. Chisti, U.C. Banerjee, Biotechnol. Adv. 31 (2013) 346–356.
[7] M.S. Aktar, J. Panwar, Y.-S. Yung, ACS Sustain. Chem. Eng. 1 (2013) 591–602.
[8] S.S. Shnakr, A. Ahmad, R. Pasricha, M. Sastry, J. Mater. Chem. 13 (2003) 1822–1826.
[9] A. Husen, M. Ghorbanpour, M. Khanuja, A. Varuna (Eds.), Nanoscience and Plant-Soil Systems, Springer, Switzerland, 2017, pp. 455–479.
[10] N. Muniyappan, N.S. Nagarajan, J. Environ. Chem. Eng. 2 (2014) 2037–2044.
[11] D.S. Sheny, J. Mathew, D. Philip, Spectrochim. Acta A 97 (2012) 306–310.
[12] A. Dzimitrowicz, S. Berent, A. Motyka, P. Jamroz, K. Kurcbach, W. Sledz, P. Pohl, Arab. J. Chem. (2016), https://doi.org/10.1016/j.arabjc.2016.09.007 in press.
[13] A. Mayoral, J. Agúndez, I.M. Pascual-Valderrama, J. Pérez-Pariente, Gold Bull. 47 (2014) 161–165.
[14] J. Agúndez, L. Martin, A. Mayoral, J. Pérez-Pariente, Catal. Today 304 (2018) 172–180.
[15] N. Lemery, *Cours de Chymie*, 1757, L.-C. d'Houry, Paris.
[16] J. Pérez-Pariente, I. Pascual-Valderrama, J. Agúndez, 9th International Conference for the History of Chemistry, Uppsala, Sweden, 2013.
[17] S.Y. Lee, S. Krishnamurthy, C.-W. Cho, Y.-S. Yun, ACS Sustain. Chem. Eng. 4 (2016)

26-51-2659.
[18] K.K.R. Datta, B.V.S. Reddy, K. Ariga, A. Vinu, Angew. Chem. Int. Ed. 49 (2010) 5961–5965.
[19] M.D. Hughes, Y.-J. Xu, P. Jenkins, P. McMorn, P. Landon, D.I. Enache, A.F. Carley, G.A. Attard, G.J. Hutchings, F. King, E.H. Stitt, P. Johnston, K. Griffin, C.J. Kiely, Nature 437 (2005) 1132–1135.
[20] D. Margolese, J.A. Melero, S.C. Christiansen, B.F. Chmelka, G.D. Stucky, Chem. Mater. 12 (2000) 2448–2459.
[21] J.P. Thielemann, F. Girgsdies, R. Schlög, C. Hess, Beilstein, J. Nanotechnol. 2 (2011) 110–118.
[22] A.C. Cattaneo, C. Ferar, D.C. Villa, S. Angioni, C. Milanese, D. Capsoni, S. Grandi, P. Mustarelli, V. Allodi, G. Mariotto, S. Brutti, E. Quatarone, Microporous Mesoporous Mater. 219 (2016) 210–220.
[23] J.D. Webb, T. Seki, J.F. Goldston, M. Pruski, C.M. Crudden, Microporous Mesoporous Mater. 203 (2015) 123–131.
[24] I. Diaz, C. Márquez-Álvarez, F. Mohíno, J. Pérez-Pariente, E. Sastre, J. Catal. 193 (2000) 283–294.
[25] A.K. Singh, O.N. Srivastava, Nanoscale Res. Lett. 10 (2015) 353.
[26] S.M. Pourmortazavi, M. Taghdiri, V. Makari, M. Rahimi-Nasrabadi, H. Batodi, Int. J. Food Prop. 20 (2017) 1097–1103.
[27] S. Link, M.A. El-Sayed, J. Phys. Chem. B 103 (1999) 4212–4217.
[28] G.H. Woehrle, M.G. Warner, J.E. Hutchinson, J. Phys. Chem. B 106 (2002) 9979–9981.
[29] N. Bogdanchikova, A. Pestryakov, I. Tuzovskaya, T.A. Zepeda, M.H. Farias, H. Tiznado, O.A. Martyniuk, Fuel 110 (2013) 40–47.
[30] D.G. Castner, K. Hinds, D.W. Grainger, Langmuir 12 (1996) 5083–5086.
[31] E. Cano-Serrano, G. Blanco-Brieva, J.M. Campos-Martin, J.L.G. Fierro, Langmuir 19 (2003) 7621–7627.
[32] M.C. Bourg, A. Badia, R. Bruce Lennox, J. Phys. Chem. B 104 (2000) 6562–6567.
[33] M. Brust, M. Walker, D. Bethell, D.J. Schiffrin, R. Whyman, J. Chem. Soc. Chem. Commun. (1994) 801–802.
[34] D.M. Cox, B. Kessler, P. Fayet, W. Eberhardt, Z. Fu, D. Sondericher, R. Sherwood, A. Kaldor, Nanostruct. Mater. 1 (1992) 161–165.
[35] S. Peters, S. Peredkov, M. Neeb, W. Eberhardt, M. Al-Hada, Surf. Sci. 608 (2013) 129–134.
[36] H. Schmidbaur, J.R. Mandl, F.E. Wagner, D.F. Van de Vondel, G.P. Van der Kelen, J. Chem. Soc. Chem. Commun. (1976) 170–172.
[37] A. McNeillie, D.H. Brown, W.E. Smith, M. Gibson, L. Watson, J. Chem. Soc. Dalt. Trans. (1980) 767–770.
[38] J.J. Pireaux, M. Liehr, P.A. Thiry, J.P. Delrue, R. Caudano, Surf. Sci. 141 (1984) 221–232.
[39] M. Haruta, S. Tsubota, T. Kobayashi, H. Kageyama, M.J. Genet, B. Delmon, J. Catal. 144 (1993) 175–192.
[40] W.S. Epling, G.B. Hoflund, J.F. Weaver, S. Tsubota, M. Haruta, J. Phys. Chem. 100 (1996) 9929–9934.
[41] E.D. Park, J.S. Lee, J. Catal. 186 (1999) 1–11.
[42] B.G. Donoeva, D.S. Ovoshchnikov, V.B. Golovko, ACS Catal. 3 (2013) 2986–2991.